HAL
open science

Neutron structure of type III Antifreeze Protein allows the reconstruction of AFP-ice interface

Eduardo Howard, Matthew Blakeley, Michael Haertlein, Isabelle Petit-Hartlein, Andre Mitschler, Stuart Fisher, Alexandra Cousido-Siah, Andres Salvay, Alexandre Popov, Christophe Muller-Dieckmann, et al.

To cite this version:

Eduardo Howard, Matthew Blakeley, Michael Haertlein, Isabelle Petit-Hartlein, Andre Mitschler, et al.. Neutron structure of type III Antifreeze Protein allows the reconstruction of AFP-ice interface. Journal of Molecular Recognition, 2011, 24 (4), pp.724. 10.1002/jmr.1130 . hal-00629934

HAL Id: hal-00629934

https://hal.science/hal-00629934v1

Submitted on 7 Oct 2011

HAL is a multi-disciplinary open access archive for the deposit and dissemination of scientific research documents, whether they are published or not. The documents may come from teaching and research institutions in France or abroad, or from public or private research centers.

L'archive ouverte pluridisciplinaire **HAL**, est destinée au dépôt et à la diffusion de documents scientifiques de niveau recherche, publiés ou non, émanant des établissements d'enseignement et de recherche français ou étrangers, des laboratoires publics ou privés.

Journal of Molecular Recognition

Neutron structure of type III Antifreeze Protein allows the reconstruction of AFP-ice interface

Journal:	*Journal of Molecular Recognition*
Manuscript ID:	JMR-10-0126.R1
Wiley - Manuscript type:	Research Article
Date Submitted by the Author:	19-Jan-2011
Complete List of Authors:	Podjarny, Alberto; IGBMC, Structural Biology Howard, Eduardo; IFLYSIB Blakeley, Matthew; ILL Haertlein, Michael; ILL, PSB Petit-Hartlein, Isabelle; IBS Mitschler, Andre; IGBMC, Structural Biology and Genomics Fisher, Stuart; ILL Cousido-Siah, Alexandra; IGBMC, Structural Biology and Genomics Salvay, Andres; IFLYSIB Popov, Alexandre; ESRF Muller-Dieckmann, Christophe; ESRF Petrova, Tatiana; IMPB
Keywords:	neutron protein crystallography, antifreeze protein

SCHOLARONE™
Manuscripts

Neutron structure of type-III Antifreeze Protein allows the reconstruction of AFP-ice interface

Eduardo I. Howard[a*], Matthew P. Blakeley[b], Michael Haertlein[b,c], Isabelle Petit-Haertlein[b,c], Andre Mitschler[d], Stuart J. Fisher[b,e], Alexandra Cousido-Siah[d], Andrés G. Salvay[a,f], Alexandre Popov[g], Christoph Muller-Dieckmann[g], Tatiana Petrova[h], Alberto Podjarny[d*]

[a]IFLYSIB, UNLP-CONICET, Calle 59, 789, B1900BTE, La Plata, Argentina
[b]Institut Laue-Langevin, 6 rue Jules Horowitz, 38042, Grenoble, France,
[c]ILL–EMBL Deuteration Laboratory, Partnership for Structural Biology, 6 rue Jules Horowitz, 38042 Grenoble, France,
[d]IGBMC, CNRS, INSERM, Université de Strasbourg, 1 rue Laurent Fries, Illkirch, France
[e]Department of Molecular Biology, Faculty of Natural Sciences, University of Salzburg, Salzburg, Austria
[f]Universidad Nacional de Quilmes, Roque Sáenz Peña 352, B1876BXD Bernal, Argentina
[g]ESRF, 6 rue Jules Horowitz, 38043, Grenoble, France
[h] Institute of Mathematical Problems of Biology, Russian Academy of Sciences, Pushchino, 142290 Russia

*Corresponding authors
howard@iflysib.unlp.edu.ar
podjarny@igbmc.fr

For Peer Review

Abstract

Antifreeze proteins (AFPs) inhibit ice growth at sub-zero temperatures. The prototypical type-III AFPs have been extensively studied, notably by X-ray crystallography, solid-state and solution NMR, and mutagenesis, leading to the identification of a compound ice-binding surface (IBS) composed of two adjacent ice-binding sections, each which binds to particular lattice planes of ice crystals, poisoning their growth. This surface, including many hydrophobic and some hydrophilic residues, has been extensively used to model the interaction of AFP with ice. Experimentally observed water molecules facing the IBS have been used in an attempt to validate these models. However, these trials have been hindered by the

limited capability of X-ray crystallography to reliably identify all water molecules of the hydration layer. Due to the strong diffraction signal from both the oxygen and deuterium atoms, neutron diffraction provides a more effective way to determine the water molecule positions (as D_2O). Here we report the successful structure determination at 293K of fully perdeuterated type-III AFP by joint X-ray and neutron diffraction providing a very detailed description of the protein and its solvent structure. X-ray data were collected to a resolution of 1.05 Å, and neutron Laue data to a resolution of 1.85 Å with a "radically small" crystal volume of 0.13 mm^3. The identification of a tetrahedral water cluster in nuclear scattering density maps has allowed the reconstruction of the IBS-bound ice crystal primary prismatic face. Analysis of the interactions between the IBS and the bound ice crystal primary prismatic face indicates the role of the hydrophobic residues, which are found to bind inside the holes of the ice surface, thus explaining the specificity of AFPs for ice versus water.

Introduction

The so-called Antifreeze Proteins (AFPs) allow certain organisms living in cold environments to survive sub-zero temperatures. They do this by preventing ice growth and recrystallization in internal fluids through binding to ice surfaces (Davies *et al.,* 2002; Margesin *et al.,* 2007; Venketesh and Dayananda, 2008). This presents a unique case of molecular recognition, as AFPs need to discriminate between ice nuclei and bulk water at slightly sub-zero temperatures, and therefore, they need to recognize local structural features of ice which are not present in liquid water (Jia and Davies, 2002).

For Peer Review

The recognition and further binding to ice is the first stage in a two-step *adsorption and growth inhibition* mechanism (Raymond and DeVries, 1977). In this model, AFP molecules bind to well-defined sites on the ice surface. Ice may continue to grow between the adsorbed AFPs (which act as impurities), developing a curved front, which eventually leads to the termination of crystal growth, a phenomenon known as the Kelvin effect (Wilson, 1993; Kristiansen and Zachariassen, 2005).

The success of this protection strategy is illustrated by the wide distribution of AFPs in psychrophilic organisms, such as insects, plants, fungi and fish living in cold regions. Each of these groups contains proteins which have different origins, sequences and structures. In particular, five different types of polar fish AFPs have been described (Types I–IV and antifreeze glycoproteins) with a characteristic taxonomical distribution (DeVries, 1971; Ewart and Hew, 2002).

We have studied fish type-III AFP (HPLC-12 isoform), a prototypical globular AFP of 7 kDa which has been the subject of a large number of experimental and computational studies, allowing the identification of a region on the protein surface as responsible for the recognition of particular lattice planes of ice (Chen and Jia, 1999; Antson *et al.*, 2001; Siemer and McDermott, 2008; Siemer *et al.*, 2010; Garnham *et al.,* 2010). This compound ice-binding surface (IBS) is composed of two adjacent, nearly-flat surfaces inclined at approximately 150° to each other (Figure 1a). One binds the primary prismatic plane of ice; the other, the pyramidal plane. The IBS has the peculiarity of including a large proportion of hydrophobic residues (Figure 1b). This characteristic was unexpected as it went against early proposals for the interaction of AFP with ice, which were based on a hydrogen-bonding match of AFPs to the ice surface. However, this characteristic becomes reasonable in the perspective of differentiating locally the binding to ice, from that to bulk water. For the

John Wiley & Sons

For Peer Review

case of liquid water, binding is indeed dominated by hydrogen-bonding, whereas ice presents other structural features, such as the holes in the middle of six-membered water rings, which can accommodate hydrophobic residues. As proposed by modeling studies (Yang *et al.*, 1998) these interactions could play a main differentiation role, and would be complemented by hydrogen-bonds.

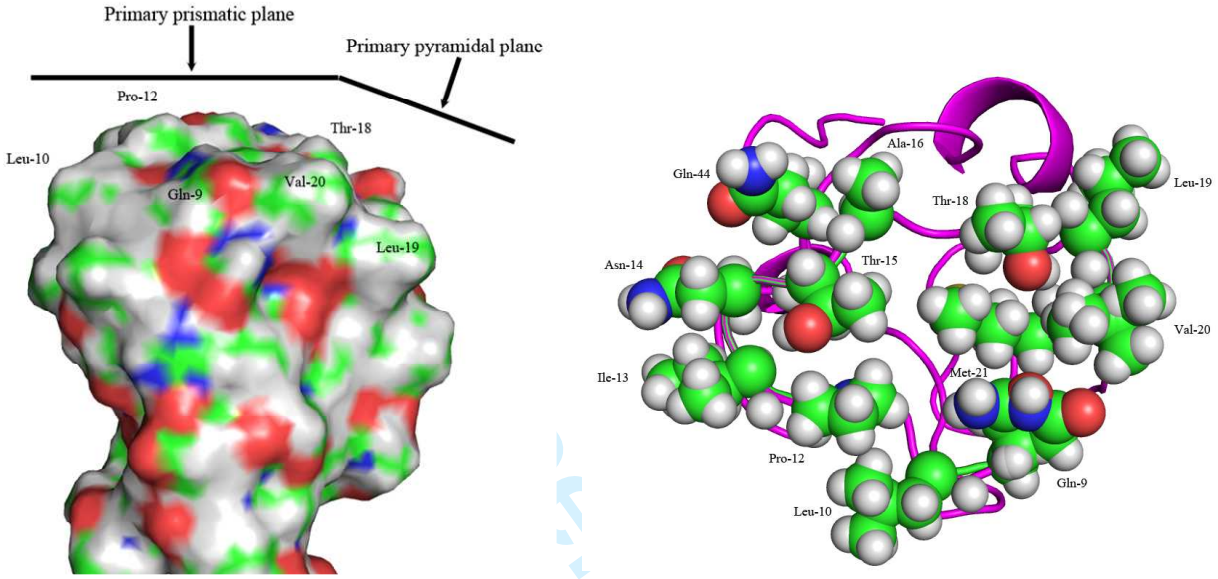

a) b)

Figure 1. a) Surface view of the compound ice-binding surface (IBS) of type-III AFP. The primary prismatic and pyramidal plane binding sections of AFP are indicated, along with some of the residues identified at the IBS (Gln-9, Leu-10, Pro-12, Thr-18, Leu-19 and Val-20). b) Ribbon representation of type-III AFP with all the compound ice-binding surface residues given as space-filled spheres (Gln-9, Leu-10, Pro-12, Ile-13, Asn-14, Thr-15, Ala-16, Thr-18, Leu-19, Val-20, Met-21, Gln-44). Residues are colored as follows: nitrogen = blue, oxygen = red, carbon = green, and deuterium = grey.

The structure of type-III AFP protein has been extensively studied, and there are about 30 models in the Protein Data Bank (http://www.rcsb.org/pdb/) that have been solved by X-ray crystallography at various levels of resolution, including structures at different pH and at different temperatures (Table I, supplementary material). Several faces of the hexagonal ice structure (prismatic, basal and others) have been fitted to

the IBS of each of these structures using modelling techniques which maximize the energy of interaction (Antson *et al*., 2001). In this study it is briefly mentioned that crystallographically observed waters are used as a hint to the position of ice water molecules. The result is a series of interface models, which explain the binding of AFP to several ice planes. These models are supported experimentally by macroscopic observations from etching experiments (Antson *et al.,* 2001; Garnham *et al.,* 2010). Nevertheless, there is no direct structural experimental evidence specifically identifying the atomic interactions of the IBS with specific water molecules in the ice planes.

In order to increase the visibility of partially disordered waters facing the IBS we have used neutron crystallographic techniques in combination with fully perdeuterated crystals of type-III AFP in heavy water (D_2O). In this way, the signal from D_2O water molecules is significantly increased (about 3 times) relative to H_2O water molecules, since deuterium atoms have a similar neutron scattering strength to carbon, nitrogen or oxygen atoms (note that deuterium atoms diffract X-rays very weakly). This is particularly useful in difficult cases where the diffraction signal is close to the noise level. In addition, neutrons do not provoke any observable crystal radiation damage, and therefore allow studies without cryo-cooling of the crystals, in conditions which are close to those *in-vivo*.

In spite of these advantages with respect to X-ray protein crystallography, fewer than 50 structures solved by neutron diffraction techniques are deposited in the Protein Data Bank (around 1/1000 of the total), mostly from partially deuterated (with only exchangeable hydrogen atoms replaced by deuterium) crystals. The reasons for this low number are that neutron sources are very few and their fluxes are relatively low,

John Wiley & Sons

For Peer Review

and therefore very large crystals (which are difficult to grow) and long data collection times (in the order of weeks) have been needed to compensate for these limitations.

Recently, the use of fully perdeuterated crystals, obtained from samples from dedicated deuteration facilities (Forsyth *et al.,* 2001), and the improvement of data collection beam-lines, have allowed the use of much smaller crystals and therefore enlarged the field of applicability of neutron diffraction to biological problems (Blakeley, 2009). This is the case in the present work, where high quality neutron data has been obtained from a radically small crystal (volume = 0.13mm^3) by neutron diffraction standards.

Materials and Methods

Production and characterization of perdeuterated type-III AFP (AFP D)

The synthetic gene of the type-III AFP corresponding to the sequence of the 1HG7 PDB entry (http://www.rcsb.org/pdb/explore/explore.do?structureId=1HG7) (Antson *et al.*, 2001) was used (Salvay *et al.,* 2007). It was over-expressed in *Escherichia coli* BL21(DE3) at the ILL-EMBL Deuteration Facility in Grenoble, France (Petit-Haertlein *et al.*, 2009). The molecular weight of AFP D and its deuteration level were determined by MALDI Mass Spectrometry. Samples of concentrated native AFP diluted in trifluoroacetic acid 0.1% (Sigma) (final concentration about 10 m*M*), were mixed with an equal volume of a saturated solution of sinapinic acid (Fluka) prepared in a 50% (*v/v*) solution of acetonitrile/aqueous 0.3% trifluoroacetic acid directly on the stainless steel sample plate and air-dried prior to analysis. The measured molecular weight obtained (7456 Da), when AFP D was refolded in H_2O buffer, is very close to

For Peer Review

the theoretical value (7452 Da), indicating that more than 99% of the 418 non-exchangeable (carbon-bound) hydrogen atoms were replaced by deuterium atoms. We conclude that AFP expressed under the conditions described above, and refolded in deuterated buffer, is fully deuterium-labeled *i.e.* perdeuterated.

Crystallization

The crystallization of AFP D in D_2O was reported previously (Petit-Haertlein *et al.,* 2009; Petit-Haertlein *et al.,* 2010). All crystallization experiments were carried out by the sitting-drop vapour-diffusion method in 24-well sitting-drop Cryschem plates (Hampton Research). The particular conditions were adapted from those of AFP H in aqueous solution by a grid search for the optimal conditions for obtaining large crystals. The differences between AFP D and AFP H crystallization conditions respectively were: (i) temperature 12°C *versus* 22°C; (ii) pH=4.8 (pD=5.2) *versus* pH=4.5; (iii) sodium acetate concentration in the reservoir 50 m*M* *versus* 20 m*M*; (iv) initial concentration of ammonium sulfate in the drop 1.5 *M* versus 1.1 *M*.

The 50µl sitting-drop was prepared at 285K using 16µl protein sample and 34µl reservoir solution and was equilibrated against 800µl reservoir solution (2.2 *M* ammonium sulfate, 9% d_8-glycerol, 50m*M* sodium acetate, pD 5.2, temperature 12°C). With these conditions, orthorhombic-shaped crystals appeared after 3 weeks and grew to maximum dimensions of 0.35 x 0.55 x 0.7 mm, corresponding to a crystal volume of 0.13mm^3.

X-ray data collection

X-ray diffraction data of perdeuterated type-III AFP crystals were measured at the ESRF beam-line ID29 at room temperature. Special care was taken to minimize the

John Wiley & Sons

For Peer Review

radiation-induced damage when collecting data at room temperature, especially as high doses of X-ray photons are needed to measure accurately the highest possible resolution data. Three crystals of the same batch with approximate dimensions of 0.2 x 0.2 x 0.6 mm were measured – the best of these provided X-ray diffraction data to a resolution of 1.05Å with adequate data processing statistics [see Table 1].

Table 1. X-ray data collection statistics for the AFP D crystal with volume of 0.024mm^3. Values in parentheses are for the highest resolution shell.

X-ray source, beam-line	ESRF, ID29
Wavelength (Å)	0.65250
Space group	$P2_12_12_1$
Unit-cell parameters	a = 32.7Å, b = 39.1Å, c = 46.5Å, α = 90°, β = 90°, γ = 90°
Resolution range (Å)	50 – 1.05 (1.09 – 1.05)
No. of observations	173588
No. of unique reflections	28534 (2819)
Completeness (%)	99.7 (99.9)
R_{merge}[#]	0.048 (0.638)
Mean $I/\sigma(I)$	32.5 (2.66)
Multiplicity	6.1

[#] $R_{merge} = \Sigma_{hkl} \Sigma_i |I_i(hkl) - \langle I(hkl)\rangle| / \Sigma_{hkl} \Sigma_i I_i(hkl)$, where $I(hkl)$ is the intensity of reflection hkl, Σ_{hkl} is the sum over all reflections and Σ_i is the sum over i measurements of reflection hkl.

Neutron data collection

Neutron quasi-Laue data were collected at 293 K on the LADI-III beam-line (Blakeley *et al.,* 2010) installed on cold neutron guide H142 at the Institut Laue-Langevin. Using the crystal of AFP D with a volume of 0.13 mm^3, diffraction data were collected to 1.85 Å resolution. As is typical for a Laue experiment, the crystal was held stationary

For Peer Review

at a different φ setting for each exposure. Initially, 13 contiguous images (Δφ = 7°) were collected using an exposure time of 24 h per image in order to collect the high-resolution data, followed by a low-resolution pass of 18 images (Δφ = 5°) using an exposure time of 2 h per image. Next, the crystal orientation was modified and a further 13 images were collected (Δφ = 7°) using an exposure time of 6 h per image, followed by 18 images (Δφ = 5°) using an exposure time of 2 h per image. Finally, the crystal orientation was modified again and a further 20 images (2h per image, Δφ = 5°) were collected, such that the complete data set comprised 82 images with an average exposure time of 6.15h per image. The neutron Laue data images were processed using the Daresbury Laboratory *LAUE* suite program *LAUEGEN*, which was modified to account for the cylindrical geometry of the detector (Campbell *et al.*, 1998). The program *LSCALE* (Arzt *et al.*, 1999) was used to determine the wavelength-normalization curve using the intensities of symmetry-equivalent reflections measured at different wavelengths and to apply wavelength-normalization calculations to the observed data. The data were then scaled and merged in *SCALA* (Collaborative Computational Project, Number 4, 1994). Data collection statistics are summarized in Table 2.

For Peer Review

Table 2. Neutron quasi-Laue data collection statistics for the AFP D crystal with volume of 0.13mm^3. Values in parentheses are for the highest resolution shell.

Neutron source, guide, instrument	Institut Laue-Langevin, Cold neutron guide H142, LADI-III
Wavelength (Å)	3.18 – 4.22
No. of images	82
Image width	Stationary
Setting spacing (°)	5, 7
Average exposure time (h)	6.15
Space group	$P2_12_12_1$
Unit-cell parameters	a = 32.7Å, b = 39.1Å, c = 46.5Å, α = 90°, β = 90°, γ = 90°
Resolution range (Å)	32.74 – 1.85 (1.95 – 1.85)
No. of observations	71182 (3133)
No. of unique reflections	4803 (544)
Completeness (%)	89.3 (71.4)
R_{merge}[#]	0.140 (0.195)
$R_{p.i.m.}$(all I^+ and I^-)[§]	0.031 (0.069)
Mean $I/\sigma(I)$	17.5 (5.5)
Multiplicity	14.8 (5.8)

[#] $R_{merge} = \Sigma_{hkl} \Sigma_i |I_i(hkl) - \langle I(hkl)\rangle| / \Sigma_{hkl} \Sigma_i I_i(hkl)$, where $I(hkl)$ is the intensity of reflection hkl, Σ_{hkl} is the sum over all reflections and Σ_i is the sum over i measurements of reflection hkl.

[§] $R_{p.i.m.} = \Sigma_{hkl} [1/(N-1)]^{1/2} \Sigma_i |I_i(hkl) - \langle I(hkl)\rangle| / \Sigma_{hkl} \Sigma_i I_i(hkl)$ (Weiss, 2001), where $I(hkl)$ is the intensity of reflection hkl, Σ_{hkl} is the sum over all reflections and Σ_i is the sum over i measurements of reflection hkl.

For Peer Review

X-ray structure determination and refinement

The D AFP structure was initially solved by molecular replacement using the PDB entry 1UCS (Ko *et al.*, 2003) and the program AMoRe (Navaza, 1994). The structure was initially refined in a single conformation mode against the X-ray data alone using the program REFMAC5 (Murshudov *et al.*, 1997) to an R_{work} of 18.7 % and an R_{free} of 21.2 % to 1.05Å resolution.

Joint X+N refinement

The single conformation X-ray structural model of AFP D to 1.05Å resolution determined at room-temperature was used as the starting model for the refinement using both the X-ray and neutron data in a joint refinement strategy using the *phenix.refine* program (Afonine *et al.,* 2010) in PHENIX (version 1.6.2). The model was first modified by removing all water molecules, and then random atom shifts (0.2 Å) were applied to the coordinates. Deuterium atoms where then added to the protein model using the *ReadySet!* program in the PHENIX program suite. Initially rigid-body refinement was performed, followed by several cycles of maximum-likelihood-based refinement of individual coordinates, atomic displacement parameters (ADPs) and atomic occupancies (isotropic for D-atoms, anisotropic for all other atoms). Using the modeling program *Coot* (Emsley *et al.,* 2010), rotamer and torsion angle adjustments were made manually throughout the model according to positive nuclear scattering density in both σ_A-weighted $2F_o - F_c$ and $F_o - F_c$ maps. The N-terminal methionine residue was seen to be disordered in the nuclear scattering density maps and could not be modeled. D_2O molecules were added to the model according to positive nuclear density in σ_A-weighted $F_o - F_c$ maps, with manual adjustment of all D_2O molecules completed using both σ_A-weighted $2F_o - F_c$ and $F_o - F_c$ nuclear scattering

For Peer Review

density maps. A total of 73 solvent molecules were included in the final round of refinement using *phenix.refine*; 64 of these could be modeled as full D_2O molecules, with another 9 exhibiting spherical nuclear density and hence were modeled as O-only. The neutron R_{work} and R_{free} values for the final model were 16.2% and 21.6%, respectively, while the X-ray R_{work} and R_{free} values were 15.7% and 18.2%, respectively. The final refinement statistics from *phenix.refine* are summarized in Table 3. Molprobity (Davis *et al.,* 2007) was used to analyze the stereochemistry of the final model (see Table 3).

Table 3. Joint X-ray and neutron refinement statistics.

Refinement	Neutron	X-ray
Resolution range (Å)	29.95 – 1.85	19.6 – 1.05
R_{work} (%)	16.2	15.7
R_{free} (%)	21.6	18.2
No. of reflections	4792	28514
Model		
$RMSD_{bonds}$ (Å)	0.012	
$RMSD_{angles}$ (°)	1.35	
Atoms	1290	
Solvent molecules	73 (64 D_2O, 9 O-only)	
Deuterium atoms	689	
Residues with alternate conformations	Gln-9, Val-20, Glu-25, Thr-28, Asp-36, Val-45, Leu-55	
Ramachandran plot		
Favoured (%)	98.6	
Outliers (%)	0	
Rotamer outliers (%)	0	
Accepted regions (%)	1.4	

For Peer Review

Results: Description of the joint X-ray/neutron structure

In this work, we have used joint neutron and X-ray diffraction data to obtain a very complete description of the AFP structure, including the positions of all deuterium atoms of both the protein and ordered water molecules. Examples of the high quality nuclear scattering density maps are illustrated in Figures 2 and 3, for the protein and solvent respectively.

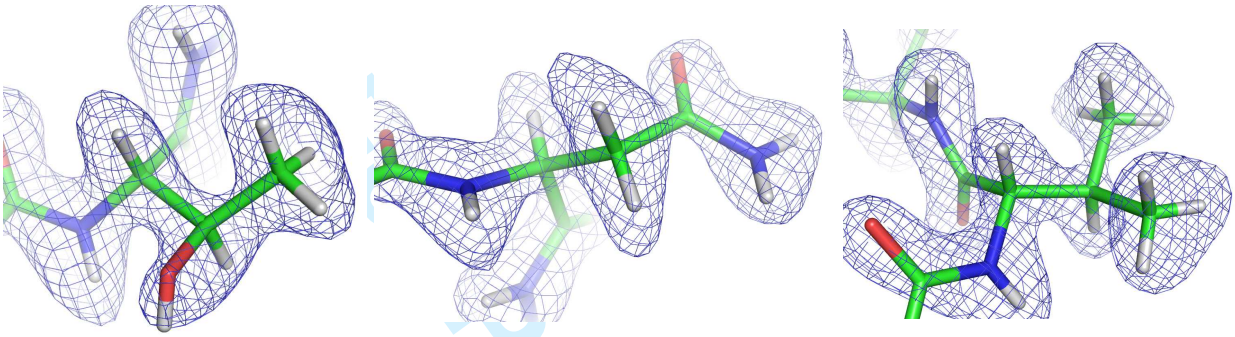

a) b) c)

Figure 2. σ_A-weighted $2F_o - F_c$ nuclear scattering density maps (contour level = 1.6 r.m.s.) for AFP D at 1.85Å resolution. a) Threonine-53. b) Asparagine-8. c) Valine-5. The orientations of the side-chains of amino-acid residues (*e.g.* methyl- and hydroxyl groups) are clearly seen due to the high quality of the nuclear scattering density maps obtained when using perdeuterated samples for data collection.

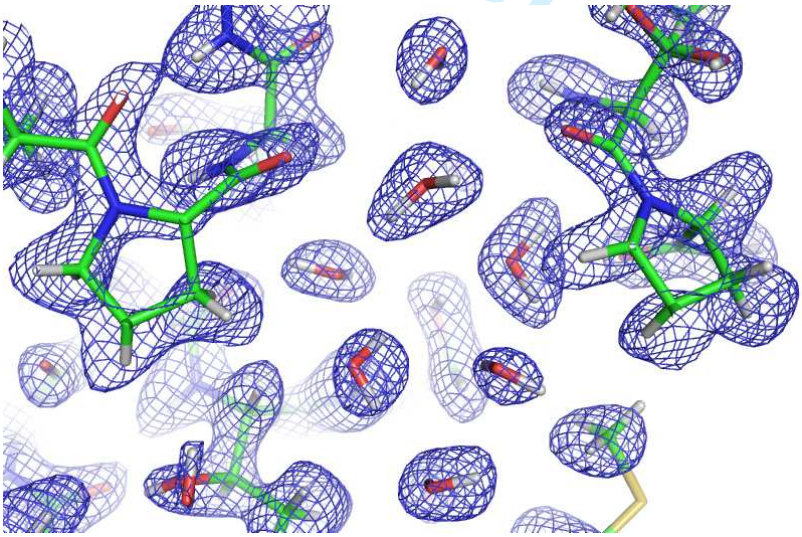

Figure 3. σ_A-weighted $2F_o - F_c$ nuclear scattering density map (contour level = 1.5 r.m.s.) for a water-cluster away from the IBS and located between two proline residues (Pro-29 & Pro-57). Note that both the O and D atoms are clearly seen in the map, showing the water molecule positions and their orientations.

A comparison between the present work and the previously published type-III AFPs shows that the protein structure is essentially conserved. However, the joint X+N refinement leads to a more complete description of the hydration layer, including both ordered (64 D_2O molecules) and slightly disordered waters (9 O-only), which are difficult to see with X-ray diffraction. Note that disordered water molecules do not contribute to high-resolution diffraction, and therefore this difficulty is not overcome by obtaining very high resolution X-ray data.

Identification of the tetrahedral water

From analysis of the nuclear scattering density maps for the solvent structure, we were able to identify a cluster of four water molecules bound to a pocket in the IBS (Figure 4) formed by Gln-9, Thr-18, Val-20 and Met-21. This water cluster was seen to be close to tetrahedral geometry with one of the water molecules (1004) clearly more disordered than the three others (Figure 5a). Upon close examination of the X-ray maps for this disordered water, two positions (1004A and 1004B) could be modeled (Figure 5b) indicating a split water position, with one of them (1004A) being in almost perfect tetrahedral geometry. The fact that this water has a split conformation and a relatively weak signal explains why it has been overlooked by previous structure determinations. Note also that this water cluster is observed in a region accessible to the solvent, while other parts of the IBS are involved in intermolecular contacts in the crystal and therefore possible similar clusters cannot be observed as the accessible surface is blocked by neighbouring molecules.

For Peer Review

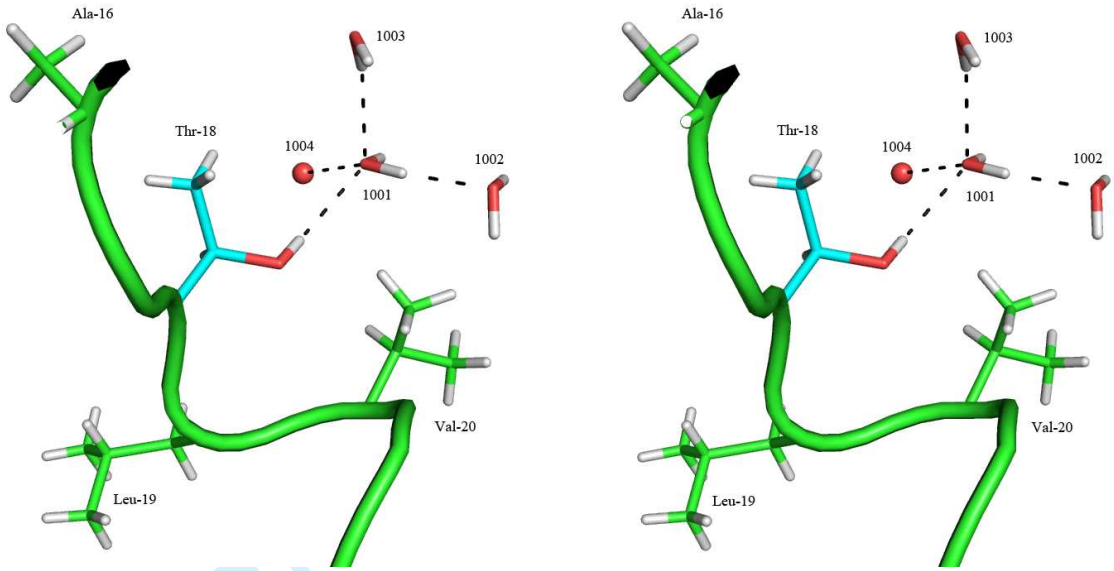

Figure 4. Stereo view of the tetrahedral water cluster bound to a pocket in the IBS. Some of the side-chains of amino-acid residues (Ala-16, Thr-18, Leu-19 and Val-20) in the vicinity of the water cluster are shown also.

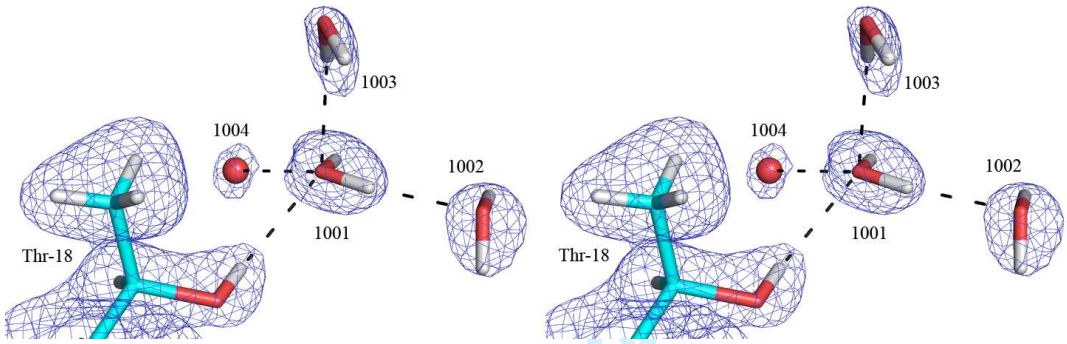

a)

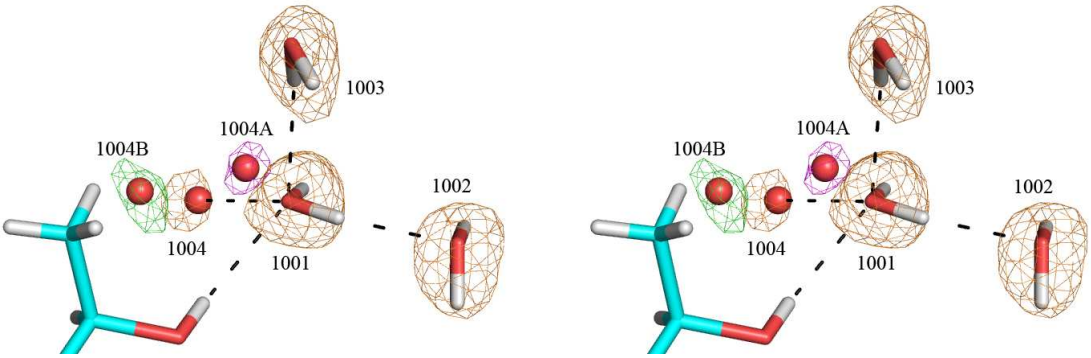

b)

Figure 5. Superposition of the tetrahedral water cluster model and density maps.

a) In blue, the σ_A-weighted $2F_o - F_c$ nuclear scattering density map (contour level = 1 r.m.s.) for the tetrahedral water cluster. Note that while there are large nuclear scattering peaks for the three water molecules 1001, 1002 and 1003, the nuclear scattering peak for water

1004 is much weaker, indicating disorder – as such it can only be modeled as an oxygen atom.
b) In orange, the σ_A-weighted $F_o - F_c$ omit nuclear scattering density map (contour level = 2.6σ) for the tetrahedral water cluster, showing the strong signal for three of the four water molecules (1001, 1002, 1003) and a relatively weaker signal for the disordered water 1004. From analysis of the room temperature X-ray data for this tetrahedral water cluster, the water identified as disordered in the nuclear scattering density maps (1004) is found to be disordered in the electron density maps also. The electron density maps indicate that this water is in a split conformation, with the 2 sites (1004A and 1004B) located either side of the position identified from the nuclear scattering density maps (1004). In magenta, the σ_A-weighted $F_o - F_c$ electron density map (contour level = 2.6σ) showing the peak for the first position 1004A of the disordered water. The position of 1004A is seen to be in ideal tetrahedral geometry for the water cluster. In green, the σ_A-weighted $F_o - F_c$ electron density map (contour level = 2.6σ) showing the peak for the second position 1004B of the disordered water.

Ice Model building

The tetrahedral water cluster was then used to fit a primary prismatic plane of ice to the protein. This was done by simple least-squares superposition using the CCP4 program LSQKAB (Kabsch, 1976; see figure 1S). Three waters of the tetrahedral cluster were then expanded to a six member water ring, which is the basic building block of the hexagonal ice structure. When doing this expansion, there are two possibilities for the water ring conformation: (1) boat or (2) chair. The boat conformation clearly placed the primary prismatic face roughly parallel to the orientation of the IBS plane and therefore was chosen as the most plausible orientation (Figure 6). The chair conformation placed the basal face roughly parallel to the IBS plane. It should be noted that the fit between a complete ice face and the IBS is not perfect, as there are short contacts between Pro-12 (which protrudes slightly from the IBS plane) and the ice faces (Figure 7).

For Peer Review

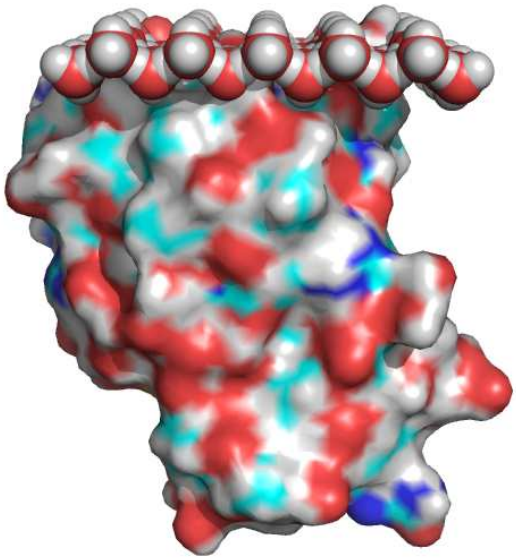

Figure 6. Primary prismatic ice face bound to the IBS in type-III AFP, built by expansion of the experimentally determined positions of the tetrahedral water cluster.

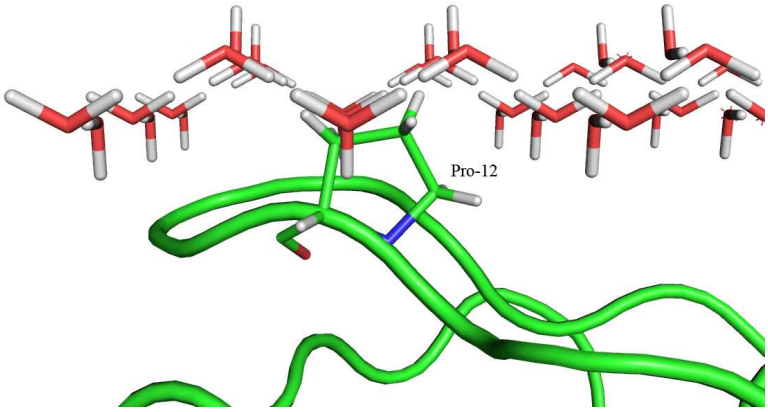

Figure 7. A close-up of the superposed prismatic plane of ice interaction with the IBS, illustrating the short contacts between Pro-12 and the ice face (other side chains have been removed for clarity).

Analysis of the ice model

From inspection of the AFP-ice interaction it could be clearly seen that the hydrophobic patches (such as the methyl groups of Thr-18, Val-20, Met-21) at the IBS face the holes in the middle of the ice water rings (Figure 8). This is in agreement

with the NMR observation (Siemer and McDermott, 2008) that these hydrophobic residues make strong van der Waals interactions with ice, necessitating a large interaction surface that can be provided by burying these residues in the water rings. The ice waters resulting from this model show clear H-Bond interactions with the polar IBS residues. The van der Waals interactions observed here are similar to those in water clathrate-protein interactions, such as those identified in crambin (Teeter *et al.,* 2001), however, in the AFP-ice case the van der Waals interactions are made with the six-membered rings of the ice structure, while in water clathrate-protein interactions the van der Waals interactions are more commonly observed for pentagonal arrangements of water molecules.

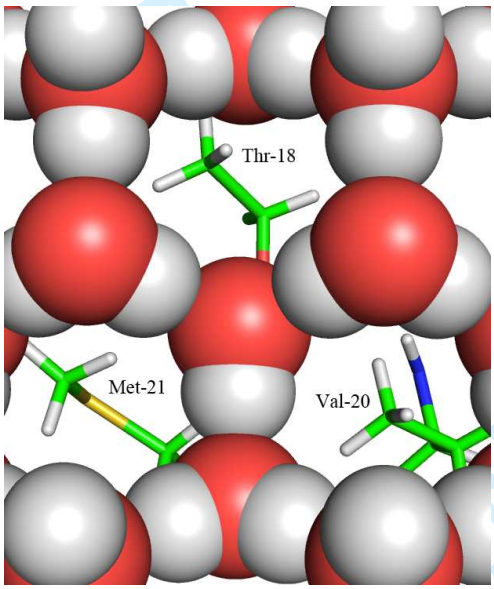

Figure 8. Detail of the interface showing the methyl groups of the hydrophobic residues Thr-18, Val-20 and Met-21 are placed facing the holes in the ice structure.

Discussion

We have determined the structure of type-III AFP and its hydration layer using joint neutron and X-ray diffraction data to obtain a maximum signal for the water molecules. Within the solvent structure we have been able to identify a water cluster with a tetrahedral geometry, typical of ice crystals. We have made the assumption

that this water cluster corresponds to the binding of type-III AFP to ice nuclei, and we have built a model of the interface of the IBS with the primary prismatic face of ice by extending this tetrahedral ice water cluster and its environment. This resulted in a model which explains the importance of the hydrophobic patches at the IBS, as they are placed facing the holes in the ice structure in the middle of the six-membered water rings and therefore can make strong van der Waals contacts with ice.

It should be noted that one of the waters in the tetrahedral cluster is more disordered, which has probably prevented the previous identification of this tetrahedral arrangement, and that some of the IBS residues, notably Pro-12, disrupt the prismatic face continuity. On the other hand, the position of Pro-12 could favor the binding of the pyramidal face as proposed by Garnham *et al.,* 2010 (Fig 1a). A key question is the reliability of the positioning of the tetrahedral water (1004A) facing the IBS. To verify this hypothesis, we analyzed all related structures of type-III AFP's deposited crystallographically determined and currently in the PDB (18 in total, see Table 1S). The positions of the water molecules described in this paper were compared with those observed in these structures.

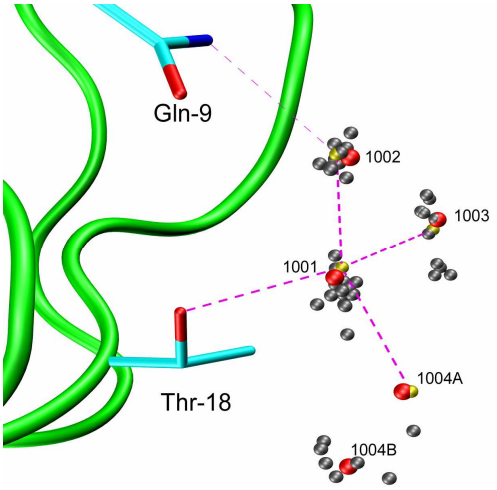

Figure 9. Comparison of tetrahedral waters with those observed in similar structures deposited in the PDB. The waters observed in this paper are

John Wiley & Sons

shown as red spheres, the superposed tetrahedral ice cluster is shown as yellow spheres (see figure 1S, supplementary material), and the waters from related PDB structures are shown as grey spheres.

The positions of the water molecules described in this paper were compared with those observed in similar protein structures deposited in the PDB (Figure 9, and figures 2S and 3S in supplementary material). Note that PDB observed water molecules which make direct protein contacts are well represented and tightly clustered around the tetrahedral positions (1001 and 1002). On the other hand, those corresponding to water 1003 are more disperse. The fourth position (1004) is the least represented and most disperse, agreeing with the double conformation that we observe. Of the two positions, 1004A and 1004B, the one with higher occupation (1004B) is the most represented in the PDB.

Conclusions

The main structural question posed by the AFP biological function is how the protein binds preferentially to ice than to water. Type-III AFP is highly soluble and does not aggregate even at high concentrations (Salvay *et al.*, 2010), so in solution it is surrounded by liquid water. On the other hand, it has a unique IBS surface, which in the presence of ice nuclei recognizes the structural features which do not exist in liquid water. Clear examples of such unique features are the holes in the centre of the water rings of ice.

Our proposition is that the IBS face of type-III AFP uses these holes to specifically recognize ice against cold but liquid water, which has a short-range order similar to ice but in which the holes in the middle of the six-membered water rings can be filled. Note that this feature directly follows from the fitting of the experimentally determined

For Peer Review

tetrahedral water cluster, which has been reliably determined by the joint X+N structure determination at room temperature.

This work highlights the importance of neutron diffraction to reliably identify hydration features in macromolecules, in particular those slightly disordered, based on its special property of the strong neutron diffraction signal of deuterium atoms. It should lead the way to further studies of this type, especially using the newly available spallation neutron sources and the methodological developments around them.

Acknowledgments

This work has benefitted from the activities of the DLAB consortium funded by the EU under contracts HPRI-2001-50065 and RII3-CT-2003-505925, and from UK EPSRC-funded activity within the ILL-EMBL Deuteration Laboratory under grants GR/R99393/01 and EP/C015452/1. This work was supported by the Human Frontiers Science Program grant RGP0021/2006-C, the Centre National de la Recherche Scientifique (CNRS), the Institut National de la Santé et de la Recherche Médicale, the Hôpital Universitaire de Strasbourg (H.U.S), the Université de Strasbourg, the Universidad de La Plata and the CONICET (PIP 112-200801-03247). EIH is a member of the career of Scientific Investigator of CONICET (Argentina).

References

Afonine PV, Mustyakimov M, Grosse-Kunstleve RW, Moriarty NW, Langan P, Adams PD. 2010. Joint X-ray and neutron refinement with phenix.refine. *Acta Cryst.* D**66**(Pt 11): 1153-63.
DOI:10.1107/S0907444910026582

For Peer Review

Antson AA, Smith DJ, Roper DI, Lewis S, Caves LSD, Verma CS, Buckley SL, Lillford PJ, Hubbard RE. 2001. Understanding the mechanism of ice binding by type-III antifreeze proteins. *J. Mol. Biol.* **305**: 875-889.
DOI:10.1006/jmbi.2000.4336.

Arzt S, Campbell JW, Harding MM, Hao Q, Helliwell JR. 1999. LSCALE – the new normalization, scaling and absorption correction program in the Daresbury *Laue* software suite. *J. Appl. Cryst.* **32**: 554–562.
DOI:10.1107/S0021889898015350

Blakeley MP. 2009. Neutron macromolecular crystallography. *Crystallogr. Rev.* **15**: 157–218.
DOI:10.1080/08893110902965003

Blakeley MP, Teixeira SC, Petit-Haertlein I, Hazemann I, Mitschler A, Haertlein M, Howard E, Podjarny AD. 2010. Neutron macromolecular crystallography with LADI-III. *Acta Cryst.* D**66**(Pt 11):1198-205.
DOI:10.1107/S0907444910019797

Campbell JW, Hao Q, Harding MM, Nguti ND, Wilkinson C. 1998. LAUEGEN version 6.0 and INTLDM. *J. Appl. Cryst.* **31**: 496–502.
DOI:10.1107/S0021889897016683

Chen G, Jia Z. 1999. Ice-binding surface of fish type-III antifreeze. *Biophys J.* **77**: 1602–1608.
DOI:10.1016/S0006-3495(99)77008-6

Collaborative Computational Project, Number 4. 1994. The CCP4 suite: programs for protein crystallography. *Acta Cryst.,* D**50**: 760–763.
DOI:10.1107/S0907444994003112

Davies PL, Hew CL. 1990. Biochemistry of fish antifreeze proteins. *FASEB J.* **4**: 2460–2468.
PMID: 2185972

For Peer Review

Davies PL, Baardsnes J, Kuiper MJ, Walker VK. 2002. Structure and function of antifreeze proteins. *Philos. Trans. R. Soc. Lond. B Biol. Sci.* **357**: 927–935.
DOI:10.1098/rstb.2002.1081

Davis IW, Leaver-Fay A, Chen VB, Block JN, Kapral GJ, Wang X, Murray LW, Arendall WB, Snoeyink J, Richardson JS, Richardson DC. 2007. MolProbity: all-atom contacts and structure validation for proteins and nucleic acids. *Nucleic Acids Res.* **35**: W375–W383.
DOI:10.1093/nar/gkm216

DeLano WL. 2008. The PyMOL molecular graphics system. DeLano Scientific LLC, Palo Alto, CA, USA. http://www.pymol.org.

DeVries AL 1971. Glycoproteins as biological antifreeze agents in Antarctic fishes. *Science* **172**: 1152–1155.
DOI:10.1126/science.172.3988.1152

Emsley P, Lohkamp B, Scott WG, Cowtan K. (2010). Features and development of Coot. *Acta Cryst.* D**66**(Pt 4):486-501.
DOI:10.1107/S0907444910007493

Ewart KV, Hew CL. 2002. *Fish antifreeze proteins*. World Scientific: London
ISBN: 9789810248994

Forsyth VT, Myles DAA, Timmins PA, Haertlein M. 2001. Possibilities for the Exploitation of Biological Deuteration in Neutron Scattering. In *Opportunities for Neutron Scattering in the 3rd Millennium*, Dianoux J (Ed) Grenoble: Institut Laue-Langevin; 47-54.

Garnham CP, Natarajan A, Middleton AJ, Kuiper MJ, Braslavsky I, Davies PL. 2010. Compound ice-binding site of an antifreeze protein revealed by mutagenesis and fluorescent tagging. *Biochemistry*. **49**: 9063-9071.
DOI:10.1021/bi100516e

For Peer Review

Jia Z, Davies PL. 2002. Antifreeze proteins: an unusual receptor-ligand interaction. *Trends Biochem. Sci.* **27**: 101-106.
DOI:10.1016/S0968-0004(01)02028-X.

Kabsch W. 1976. A solution for the best rotation to relate two sets of vectors. *Acta. Cryst.* A**32**: 922-923.
DOI:10.1107/S0567739476001873

Kristiansen E, Zachariassen KE. 2005. The mechanism by which fish antifreeze proteins cause thermal hysteresis. *Cryobiology* **51**: 262-280.
DOI:10.1016/j.cryobiol.2005.07.007

Ko T-P, Robinson H, Gao Y-G, Cheng C-HC, DeVries AL, Wang AH-J. 2003. The Refined Crystal Structure of an Eel Pout Type-III Antifreeze Protein RD1 at 0.62-Å Resolution Reveals Structural Microheterogeneity of Protein and Solvation. *Biophys. J.* **84**: 1228-1237
DOI:10.1016/S0006-3495(03)74938-8

Margesin R, Neuner G, Storey KB. 2007. Cold-loving microbes, plants, and animals - fundamental and applied aspects. *Naturwissenschaften* **94**: 77-99.
DOI:10.1007/s00114-006-0162-6

Murshudov GN, Vagin AA, Dodson EJ. 1997. Refinement of Macromolecular Structures by the Maximum-Likelihood Method. *Acta Cryst.* D**53**: 240-255.
DOI:10.1107/S0907444996012255

Navaza J. 1994. *AMoRe*: an automated package for molecular replacement. *Acta Cryst.* A**50**: 157-163.
DOI:10.1107/S0108767393007597

Petit-Haertlein I, Blakeley MP, Howard E, Hazemann I, Mitschler A, Haertlein M, Podjarny A. 2009. Perdeuteration, purification, crystallization and preliminary neutron diffraction of an ocean pout type-III antifreeze protein. *Acta Cryst.* F**65**: 406-409.
DOI:10.1107/S1744309109008574

For Peer Review

Petit-Haertlein I, Blakeley MP, Howard E, Hazemann I, Mitschler A, Podjarny A, Haertlein M. 2010. Incorporation of methyl-protonated valine and leucine residues into deuterated ocean pout type-III antifreeze protein: expression, crystallization and preliminary neutron diffraction studies. *Acta Cryst.* F**66**: 665-669.
DOI:10.1107/S1744309110012352

Raymond JA, DeVries AL. 1977. Adsorption inhibition as a mechanism of freezing resistance in polar fishes. *Proc. Natl. Acad. Sci. USA.* **74**: 2589–2593.
PMID: 267952

Salvay AG, Santos J, Howard EI. 2007. Electro-optical properties characterization of Fish Type-III Antifreeze Protein. *J. Biol. Phys.* **33**: 389-398.
DOI:10.1007/s10867-008-9080-5

Salvay AG, Gabel F, Pucci B, Santos J, Howard EI, Ebel C. 2010. Structure and interactions of fish type-III antifreeze protein in solution. *Biophys. J.* **99**: 609-618. DOI:10.1016/j.bpj.2010.04.030.

Siemer AB, McDermott AE. 2008. Solid-State NMR on a Type-III Antifreeze Protein in the Presence of Ice. *J. Am. Chem. Soc.* **130**: 17394-17399.
DOI:10.1021/ja8047893

Siemer AB, Huang K-Y, McDermott AE. 2010. Protein-ice interaction of an antifreeze protein observed with solid-state NMR. *Proc. Natl. Acad. Sci. USA*. **107**: 17580-17585.
DOI: 10.1073/pnas.1009369107

Teeter MM, Yamano A, Stec B, Mohanty U. 2001. On the nature of a glassy state of matter in a hydrated protein: Relation to protein function. *Proc. Natl. Acad. Sci. USA.* **98**(20):11242-11247.
DOI:10.1073/pnas.201404398

Venketesh S, Dayananda C. 2008. Properties, potentials, and prospects of antifreeze proteins. *Crit. Rev. Biotechnol.* **28**: 57–82.

For Peer Review

DOI:10.1080/07388550801891152

Weiss MS. 2001. Global indicators of X-ray data quality. *J. Appl. Cryst.* **34**: 130–135. DOI:10.1107/S0021889800018227

Wilson PW. 1993. Explaining thermal hysteresis by the Kelvin effect. *Cryo-Letters* **14**: 31-36.

Yang DSC, Hon W-C, Bubanko S, Xue Y, Seetharaman J, Hew CL, Sicheri F. 1998. Identification of the ice-binding surface on a type-III antifreeze protein with a “flatness function” algorithm. *Biophys J.* **74**: 2142-2151. DOI:10.1016/S0006-3495(98)77923-8

For Peer Review